Article

Study on the Bearing Capacity of the Polyethylene Pipe–Cured-In-Place Pipe Liner Composite Structure under External Pressure

Xinyi Wang, Cong Zeng, Xuefeng Yan *[ID] and Peng Zhang

Faculty of Engineering, China University of Geosciences, Wuhan 430074, China; 20221207@cug.edu.cn (X.W.);
zegncong1981@cug.edu.cn (C.Z.); cugpengzhang@cug.edu.cn (P.Z.)
* Correspondence: cugyanxf@163.com

Abstract: Cured-in-place pipe (CIPP) technology is used to repair deformed municipal polyethylene (PE) pipes caused by design flaws, construction issues, or external loads. However, research on CIPP for PE pipes is limited, restricting its broader application. This research focuses on the mechanical response characteristics and failure modes of the composite PE pipe–CIPP liner structure under external loads. Using experimental setups involving comparative test groups with different diameters and wall thickness ratios (DR values, defined as the ratio of the pipe's outer diameter to its wall thickness), this study evaluates the effects of the liner's elastic modulus, the bonding effectiveness at the PE pipe–CIPP liner interface, and the initial ovality of the pipes on the load-bearing capacity. The experimental results reveal that CIPP liners substantially enhance the stiffness and load-bearing capacity of PE pipes, with improvements ranging from 200% to nearly 500% depending on the pipe's DR value. A novel ring stiffness prediction model is also introduced and validated against the experimental data. This model provides a theoretical framework for understanding the complex interactions at the PE pipe–CIPP liner interface and aids in designing more resilient urban drainage systems.

Keywords: PE pipes; CIPP liner; bearing capacity; composite structure

1. Introduction

The rapid advancement of urbanization in China has significantly accelerated the construction of water supply and drainage pipelines, increasing the demands for the discharge of domestic sewage and industrial wastewater. By the end of 2022, the cumulative length of urban drainage networks in China exceeded 910,000 km, with annual sewage discharge surpassing 638×10^9 m³ (MHURD, 2022) [1] (Figure 1). Among these, PE pipes, due to their excellent corrosion resistance, high toughness, light weight, and cost-effectiveness, have been widely utilized in the construction of drainage networks (Soonyu Yu et al., 2015 [2]). However, factors such as design flaws, improper construction, or changes in external load conditions have led to or potentially will cause deformation defects in some buried PE pipes, which may trigger urban road surface collapses and other disasters. Accurately assessing the external pressure-bearing performance of existing buried PE pipes and enhancing the overall stability of the pipeline structure are critical issues that urgently need to be addressed.

Due to differing material properties, the mechanical response characteristics of flexible pipes under the same load conditions differ significantly from rigid pipes. Spangler (1941) [3] first proposed a method for calculating the deformation of buried flexible pipes, introducing the renowned Iowa formula. He hypothesized that the lateral soil pressure exerted on the pipe wall is proportional to the pipe sidewall thickness, and proposed a constant for the modulus of passive soil resistance. Watkins (1958) [4] considered the soil modulus at the pipe sides and revised Spangler's Iowa formula, making it widely used for calculating the deformation of flexible pipes. Spangler (1982) [5] further considered

that yielding of the side soil under horizontal pressure leads to continuous deformation of the pipe, and introduced the deformation lag coefficient in the design of buried flexible pipes. This consideration made the design of flexible pipes more aligned with actual engineering conditions, enhancing the accuracy and reliability of the design. Howard (1981) and Jeyapalan et al. (1986, 1987) [6–8] further refined and perfected Spangler's formula. Cholewa et al. (2009) [9] found that controlled pipe bursting minimally impacts nearby PVC pipes, while Saiyar et al. (2016) [10] revealed that models for stiff pipelines overestimate strains in flexible ones. Ni et al. (2018) [11] used numerical methods to develop fragility curves for pipelines affected by landslides, showing the effectiveness of simplified 2D models. Liu et al. (2023) [12] demonstrated that existing design guidelines inaccurately predict soil resistance and yield displacement for UPVC pipes under lateral movements, proposing a new method for better strain prediction. These studies collectively call for revised design practices to ensure the structural integrity of various pipeline types under diverse ground movement conditions. Through theoretical derivation, experiments, and numerical simulations, they deeply explored the deformation mechanisms and influencing factors of flexible pipes, providing more scientific and systematic guidance for the design and optimization of flexible pipes.
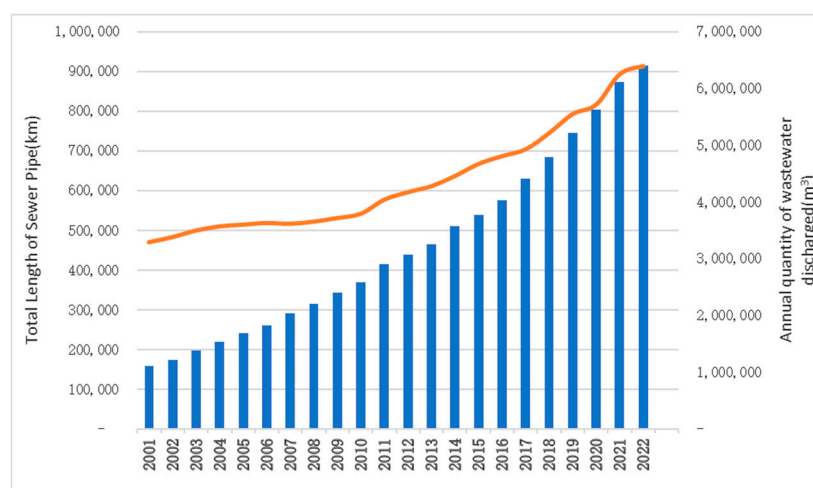
Figure 1. The length of drainage pipes in China.

The cured-in-place pipe (CIPP) trenchless rehabilitation technology allows for the installation of a closely bonded, glass fiber-reinforced resin liner within existing pipelines without excavation. This process forms a composite structure of the CIPP liner and the original pipe, jointly bearing external loads and enhancing the load-bearing capacity of PE pipes. Researchers globally have conducted theoretical studies, physical model tests, and numerical simulations to investigate the load-bearing response of pipe-liner composite structures. Takahashi et al. (2002) and Gumble et al. (2003) [13,14] demonstrated through model and full-scale tests that the CIPP liner, when integrated with the original rigid pipe, enhances the composite structure's circumferential stiffness, reducing vertical deformation under radial loads. Hsu et al. (2002) [15] utilized CIPP to rehabilitate RCP pipes in laboratory conditions, verifying that it restores the pipe's original functionality and improves hoop strength. Allouche et al. (2014) [16] explored the performance of aging steel pipes repaired with CIPP under long-term cyclic pressure, discovering that the liner's effective stiffness depends on the lesser of the composite material's circumferential and axial stiffness. Zhang et al. (2002) [17] used large-scale full-scale tests to study the mechanical characteristics of underground corroded concrete pipes repaired by spraying under combined loads. Argyrou et al. (2018) [18] examined the deformation mechanism of CIPP-reinforced defective pipes under seismic forces through full-scale tests and finite element simulations, revealing the relationship between liner interface bond failure and internal pipe pressure. Shou et al. (2020) [19] combined laboratory tests and numerical

simulations, finding that CIPP reduces stress concentration and differential displacement near corrosion voids, thereby reinforcing damaged pipes. Yang et al. (2022) [20] developed a three-dimensional numerical model of buried concrete pipes repaired with CIPP, analyzing the impact of different loads on the composite structure's bending moment. Regarding interface interactions, Mogielski et al. (2017) and Kuliczkowski et al. (2012) [21,22] studied the bonding effects of CIPP with various pipe materials and their influence on structural load capacity and stiffness. Hu et al. (2018) [23] used carbon fiber-reinforced polymer (CFRP) liners to rehabilitate prestressed concrete cylinder pipes (PCCP), and investigated the impact of the CFRP–concrete adhesive interface on repair effectiveness through finite element modeling. Yan et al. (2022) [24] utilized digital image correlation (DIC) technology to analyze the failure delamination mechanism at the interface of reinforced concrete-PE composite pipes under load.

Current research on CIPP rehabilitation of existing pipelines primarily focuses on the deformation characteristics of the original pipelines, especially rigid ones like reinforced concrete pipes (RCPs), under external loads after being lined with CIPP. However, there is a paucity of studies on the use of CIPP for rehabilitating flexible pipes, such as polyethylene (PE) pipes, and existing design theories often overlook the load-sharing role of the original pipe. There is a lack of investigation into the coordinated deformation mechanism of the composite structure under external loads, the failure modes of the composite structure when the flexible pipe and CIPP liner bear loads, and the quantitative evaluation of the load-bearing capacity enhancement due to CIPP reinforcement for flexible pipes. Furthermore, the impact of the interface interactions between the PE pipe and the CIPP liner is often treated ambiguously in current studies. Therefore, the objectives of this study are as follows: (1) to explore the mechanical response characteristics of the PE pipe–CIPP liner composite structure, and (2) to quantitatively analyze the effects of the liner's elastic modulus, liner DR value, and initial ovality on the load-bearing capacity of the PE pipe–CIPP liner composite structure.

2. Test Design

The experiment comprises four comparative test groups: T0 serves as the control group; T1, the first test group, sets the control parameter as the dimensions of the PE pipe segment, maintaining a consistent nominal diameter and controlling the wall thickness of the PE pipe segment; T2, the second test group, sets the control parameter as the bonding effect at the interface between the PE pipe and the CIPP liner; and T3, the third test group, sets the control parameter as the initial ovality of the PE pipe. By applying loads to each test group, the ring stiffness of the standard PE pipe and the ring stiffness of the composite structure post-CIPP reinforcement were obtained. The load–displacement curves, strain patterns, and fracture conditions under flat load for each test group were recorded. The group settings of the experiments are detailed in Table 1.

Table 1. Detailed settings of the tests.

Group	Test No.	PE Pipe			Other Processing		Quantity
		DN (mm)	Length (mm)	Diameter-Thickness Ratio (DR)	Additional Treatments	CIPP Liner	
T0	PE(1)	400	300	26	/	×	3
	PE(2)	400	300	21	/	×	3
	PE(3)	400	300	17	/	×	3
T1	PE(1) + CIPP	/	300	92.5	/	√	3
	PE(2) + CIPP	/	300	92.5	/	√	3
	PE(3) + CIPP	/	300	92.5	/	√	3
T2	PE(1) + CIPP(0)	/	300	92.5	PE Film	√	1
	PE(2) + CIPP(0)	/	300	92.5	PE Film	√	1
T3	PE(2) + CIPP(5%)	/	300	92.5	5% Ovality	√	1

2.1. Test Setup

The PE pipes used in this experiment were selected in accordance with the relevant provisions of ISO 4427-2: 2019 [25] while the preparation of the CIPP liner adhered to the stipulations of ISO 11295: 2022 [26]. The test setup comprised a ring stiffness testing machine, a static stress–strain measurement system, a control system, and an industrial camera (see Figure 2).
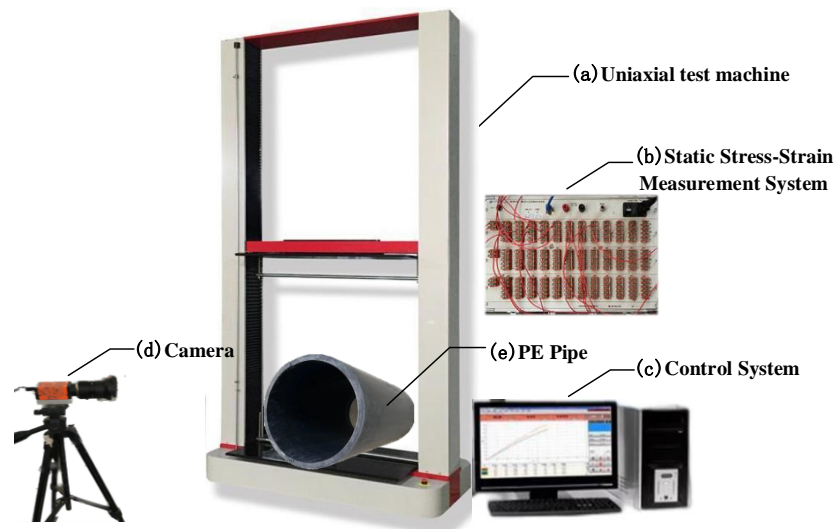

Figure 2. Test setup.

2.2. Sample Preparation

The PE pipes used for the tests were selected according to the relevant provisions of ISO 11296-3: 2018 [27]. The CIPP liner used in the tests consists of two main components: fiberglass fabric, and a resin mixture. The resin was prepared on-site by mixing polyester resin and a curing agent. The preparation process is illustrated in Figure 3:

(a) Mix resin and curing agent in a 2:1 ratio, then uniformly apply the mixture to fiberglass fabric with a density of 1050 g/m^2;

(b) Secure the impregnated hose onto an inflatable bladder, then move the bladder and hose into the pipeline to be repaired;

(c) Inflate the bladder to ensure it adheres closely to the inner wall of the pipeline;

(d) Allow it to cure at room temperature for 2 h, then release the gas and remove the bladder, trim the ends, and complete the sample preparation.
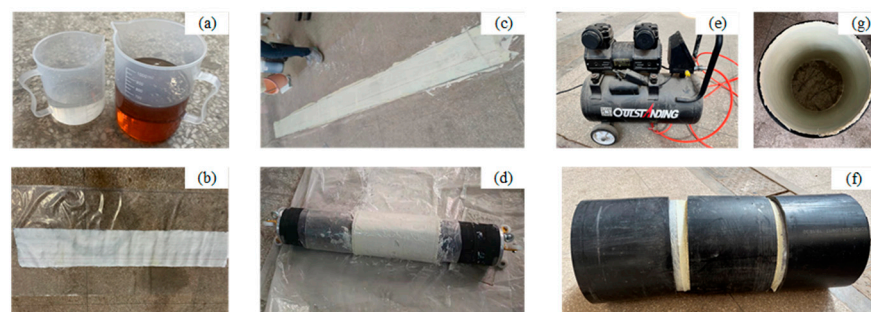
Figure 3. Specimen preparation process. (**a**) resin; (**b**) fiber-glass fabric; (**c**) apply the mixture to fiberglass fabric; (**d**) Expansion air bag; (**e**) air compressor; (**f**) PE pipe–CIPP liner; (**g**) Naturally cured CIPP liner.

2.3. Instruments

Strain gauges were employed to monitor the deformation characteristics at the inner and outer walls, as well as at the crown, bottom, and spring line of the pipe specimen during the loading process. The arrangement of the strain gauges is depicted in Figure 4. An industrial camera was positioned directly opposite the end face of the pipe specimen to capture the overall deformation process of the pipeline.
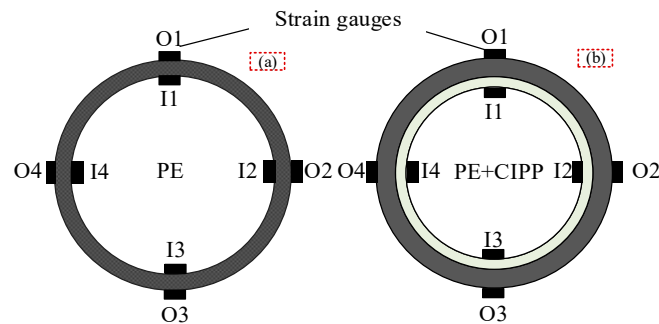
Figure 4. Instrument setup. (**a**) Original PE pipe; (**b**) PE pipe–CIPP liner.

2.4. Test Procedure

The test procedure is as follows:

(a)   Place the prepared sample on the lower plate of the ring stiffness testing machine, ensuring that the sample is in close contact with the lower plate;

(b)   Verify that the strain measurement system and the photographic system are functioning correctly;

(c)   Activate the control system, set the loading rate to 10 mm/min, and establish the loading termination condition based on a predetermined deformation in the diameter direction of the sample;

(d)   Commence loading while simultaneously recording data on load, displacement, and strain, and capture images of the deformation process with an industrial camera;

(e)   Upon reaching the predetermined conditions or upon sample failure, stop the experiment and save the data.

3. Results and Discussion

3.1. The Effect of CIPP Liner on the Enhancement of the Ring Stiffness of PE Pipe

Table 2 presents the results of the ring stiffness test for the original PE pipes and the repaired PE pipes with CIPP liner. When the outer diameter of PE pipe is the same, the smaller the DR value is, the greater its ring stiffness. After reinforcing the three types of PE pipes with varying DR values using CIPP liner, the measured the ring stiffness of PE(1) + CIPP, PE(2) + CIPP, and PE(3) + CIPP to be 21.98 kN/m^2, 41.35 kN/m^2, and 66.51 kN/m^2, respectively. It is evident that the CIPP liner significantly enhanced the bearing capacity of the PE pipe, with a DR value of 26 exhibiting a 487.7% increase, a DR value of 21 showing a 324.1% increase, and a DR value of 17 demonstrating a 295.66% increase. It was observed that when the outer diameter of the PE pipe remains constant, there is a positive correlation between the DR and the extent of load enhancement achieved through CIPP liner.

Table 2. Ring stiffness test for the original PE pipes and the repaired PE pipes with CIPP liner.

Sample Identification	Loads Corresponding to Pipes with 3.0% Deformation F (N)	3.0% Deformation of the Pipe Corresponding to the Deformation y (mm)	Test Ring Stiffness S_i (kN/m^2)	Average Ring Stiffness S (kN/m^2)	Bearing Capacity Increment (%)
PE(1)	150.89		3.56		
PE(1)	656.58	11.08	3.82	3.74	/
PE(1)	660.50		3.84		
PE(1) + CIPP-1	3540.56		21.07		
PE(1) + CIPP-2	3740.56	10.84	22.25	21.98	487.7%
PE(1) + CIPP-3	3802.25		22.62		
PE(2)	1638.88		9.74		
PE(2)	1643.12	10.85	9.77	9.75	/
PE(2)	1640.12		9.75		
PE(2) + CIPP-1	6802.32		41.31		
PE(2) + CIPP-2	6642.79	10.62	40.34	41.35	324.1%
PE(2) + CIPP-3	6982.32		42.4		
PE(3)	2752.76		16.78		
PE(3)	2758.21	10.58	16.82	16.81	/
PE(3)	2762.48		16.84		
PE(3) + CIPP-1	10,698.29		66.6		
PE(3) + CIPP-2	10,452.64	10.36	65.08	66.51	295.66%
PE(3) + CIPP-3	10,898.18		67.85		

3.2. PE Pipe and PE Pipe–CIPP Liner Failure Mode

From the experiment, it was observed that as the load increases, the PE pipe specimen undergoes oval deformation. Even with a 20% vertical deformation, no fractures occurred. Figure 5 illustrates the deformation and failure modes of the PE pipe–CIPP liner. Figure 5a depicts the initial state, with the CIPP liner bonded to the PE pipe segment. Figure 5b shows the early stage of loading, where the PE pipe–CIPP liner deforms in harmony. As loading continues, their differing stiffness prevents further coordinated deformation, leading to interface peeling and CIPP liner bulging (Figure 5c). With greater vertical deformation, the CIPP liner experiences compressive failure at the arch line, resulting in protruding layers and cracks, ultimately fracturing the CIPP liner (Figure 5d). In the later stages of loading, the interface is almost entirely detached, and the PE pipe–CIPP liner exhibits fractures at the pipe top, bottom, and arch line, with the composite structure at the top showing a tendency to split into two halves (Figure 5e). Figure 5f illustrates the fracture at the arch line of the PE pipe segment. Therefore, the failure process of the PE pipe–CIPP liner includes: ① overall coordinated deformation; ② CIPP liner peeling; ③ compressive protrusion layers at the CIPP liner arch line; and ④ pipe fracture. After unloading, the specimen rebounds, but does not fully return to its initial state.
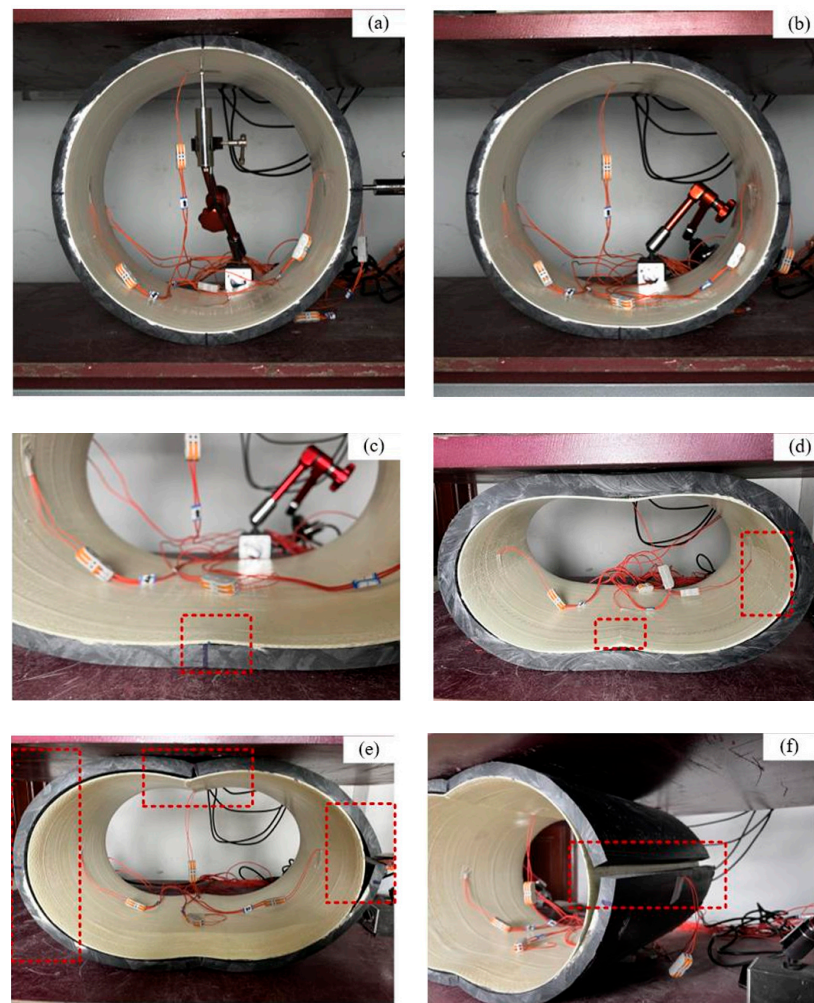
Figure 5. PE pipe and PE pipe–CIPP liner failure mode. (**a**) Initial state; (**b**) overall coordinated deformation; (**c**) interface failure; (**d**) compressive protrusion layers at the CIPP liner arch line; (**e**,**f**) PE pipe fracture.

### 3.3. The Effect of Original PE Pipe's DR on the Bearing Capacity of PE Pipe–CIPP Liner

As shown in Figure 6A, the PE pipe (DR = 26)-CIPP liner exhibited five distinct deformation stages during loading. ① *Elastic stage*: In segment O-A1, the load and displacement displayed a linear relationship; displacement increased as the load intensified. ② *Interface peeling stage*: When the load reached 8931.1 N, the specimen exhibited a vertical displacement of 33 mm, and the curve first descended at A1 to 5286.64 N, indicating partial detachment between the PE pipe segment and the CIPP liner (Figure 6A(a)). ③ *PE pipe segment failure stage*: At a load of 6173.23 N, the specimen showed a vertical displacement of 40.4 mm, with the curve descending a second time at B1 to 4899.73 N, as the PE pipe segment's top detached and cracked from the CIPP liner (Figure 6A(b)). ④ *CIPP liner failure stage*: In segment B1-C1, the displacement continued to increase, enlarging the gap between the CIPP liner and the PE pipe segment. The liner exhibited protruding layers and partial cracking of the fiberglass cloth, with the curve descending a third time at C1. The CIPP liner did not experience an instantaneous brittle fracture, showing a gradual decline past C1. ⑤ *Complete specimen failure*: At a load of 7621.77 N, the specimen displayed a vertical displacement of 111.12 mm, with the curve descending a fourth time at D1. The right side of the PE pipe segment completely fractured, and the CIPP liner ruptured and protruded, leading to the complete failure of the specimen (Figure 6A(d)).

The PE pipe (DR = 21)–CIPP liner exhibited three distinct deformation stages during loading (Figure 6B).①*Elastic stage*: In segment O-A2, the pipe segment specimen was

in the elastic stage.②*Interface failure stage*: When the load reached 11,856.54 N, the specimen showed a vertical displacement of 22.82 mm, and the curve first descended at A2 to 6588.47 N, indicating partial detachment between the CIPP liner and the PE pipe segment, but no gap was observed (Figure 6B(e)). Upon further loading to 9839.3 N, the curve descended a second time at B2 to 6588.47 N, with the CIPP liner and PE pipe segment detaching again (Figure 6B(f)). ③ *CIPP liner failure stage*: Continued loading to 7541.38 N caused the curve to descend a third time at C2 to 6381.82 N. As the load increased, a significant gap appeared at the interface between the CIPP liner and the PE pipe segment (Figure 6B(g)), and a protruding layer emerged on the inner wall at the right side of the arch line (Figure 6B(h)). By the end of the experiment, the specimen exhibited nearly 40% vertical deformation, but no cracking or other damage was observed in the PE pipe segment or the CIPP liner.
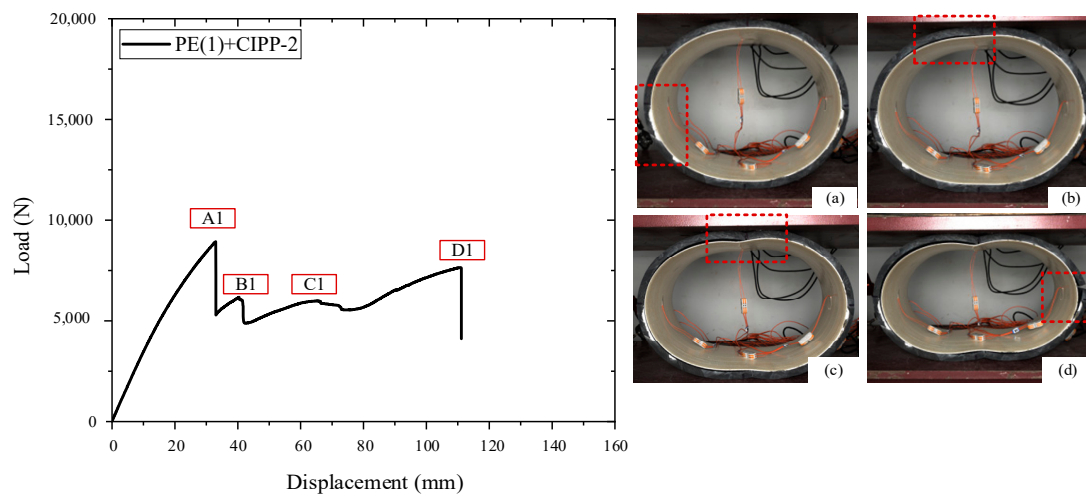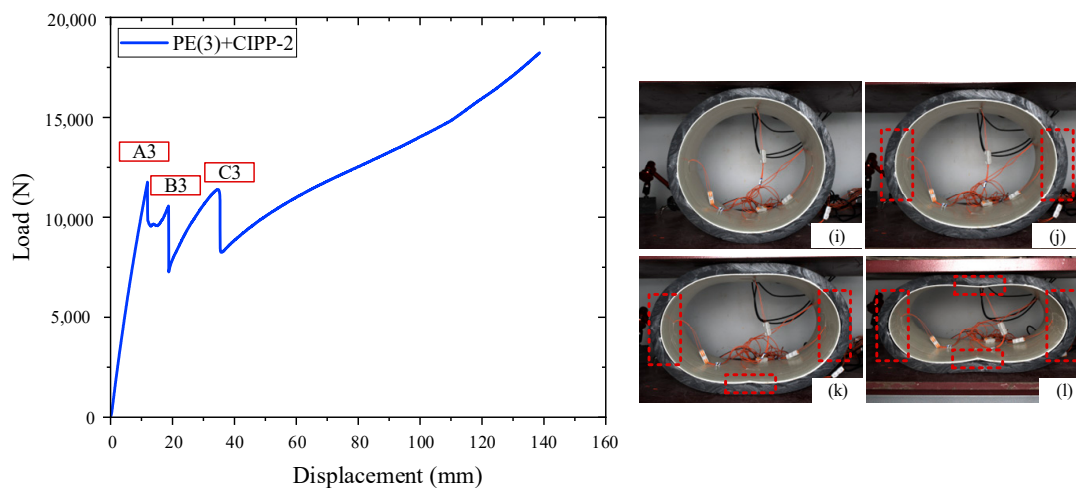

(**A**) DR = 26. (**a**) interface peeling stage; (**b**) PE pipe segment failure stage; (**c**) CIPP liner failure stage; (**d**) complete specimen failure
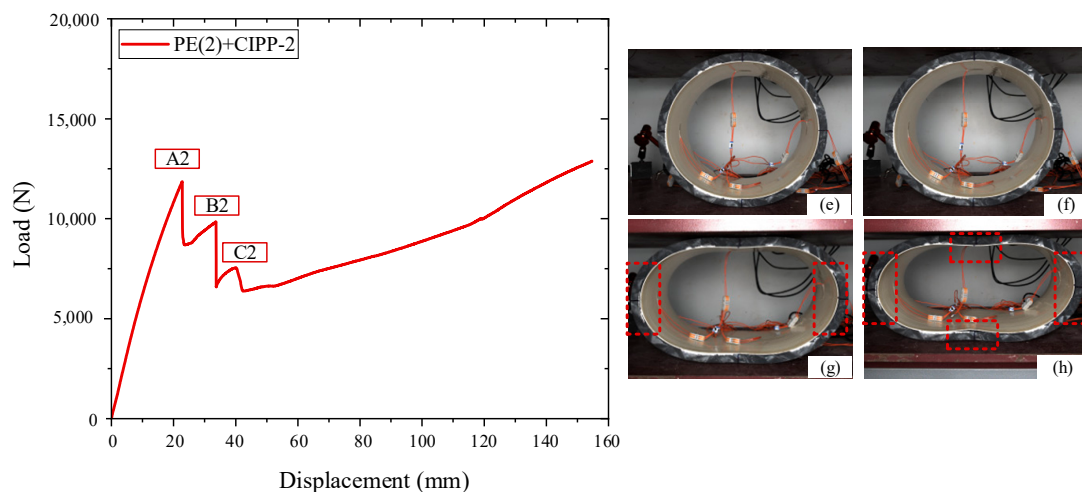
(**B**) DR = 21. (**e**) elastic stage; (**f**) interface failure stage; (**g**) CIPP liner failure stage (**h**) a protruding layer emerged on the inner wall at the right side of the arch line

Figure 6. *Cont.*

(**C**) DR = 17. (**i**) Interface failure stage; (**j**) CIPP liner failure stage; (**k**) displacement continued to rise without further points of descent; (**l**) the inner wall of the CIPP liner at the bottom of the pipe protruding and cracking.

Figure 6. Failure process of PE pipe–CIPP liner with Different DR.

The PE pipe (DR = 17)–CIPP liner exhibited three distinct deformation stages during loading (Figure 6C). ① *Elastic stage*: In segment O-A3, the pipe segment specimen remained in the elastic phase. ② *Interface failure stage*: Upon reaching a load of 11,758.6 N, the specimen exhibited a vertical displacement of 11.94 mm, with the curve initially descending at A3 to 9555.92 N, indicating partial interface failure between the PE pipe segment and the CIPP liner. Continuing to load up to 10,566.08 N resulted in a vertical displacement of 18.72 mm, with the curve descending a second time at B3 to 7268.6 N, as the interface further detached (Figure 6C(i)), although no significant gap was observed. ③ *CIPP liner failure stage*: Loading continued to 11,394.45 N, causing a vertical displacement of 34.6 mm, and the load dropped to 8244.83 N, creating annular gaps on both the left and right sides of the arch line (Figure 6C(j)). As the load increased, the displacement continued to rise without further points of descent. By the end of the experiment, the specimen exhibited 40% deformation, with the inner wall of the CIPP liner at the bottom of the pipe protruding and cracking (Figure 6C(l)), while the PE pipe segment showed no significant damage.

When the plate load is relatively low, the specimen remains in the elastic phase, with the PE pipe segment and the CIPP liner deforming in complete harmony, sharing the same neutral axis. The smaller the DR value of the PE pipe segment, the greater the increase in load-bearing capacity after repair, resulting in a corresponding larger increase in ring stiffness. As the load increases, the interface between the PE pipe segment and the CIPP liner begins to separate, leading to uncoordinated deformation. Pipe segments with smaller DR values are the first to experience interface separation. When the load-bearing capacity of the PE pipe segment is relatively poor, the PE pipe and CIPP liner crack successively, and in severe cases, they fracture directly. Conversely, when the load-bearing capacity of the PE pipe segment is stronger, the PE pipe segment does not exhibit significant damage, while the CIPP liner may show fiber protrusion or even cracking as the load increases.

3.4. The Effect of the Interface Bond on the Bearing Capacity of PE Pipe–CIPP Liner

Table 3 presents the ring stiffness test results for the group T2. The ring stiffness of the PE(1) + CIPP(0) and PE(2) + CIPP(0) pipe segment were 10.7 kN/m^2 and 23.28 kN/m^2, respectively. Comparatively, the bearing capacity of PE(1) + CIPP(0) increased by 203.12% compared to PE(1) (3.53 kN/m^2), but was lower than that of the interface-bonded PE(1) + CIPP (21.98 kN/m^2). Similarly, PE(2) + CIPP(0) showed a 138.77% increase over PE(2) (9.75 kN/m^2), yet was inferior to the interface-bonded PE(2) + CIPP (41.35 kN/m^2). This indicates that the bonding effect is crucial for enhancing the overall load-bearing capacity of the PE pipe–CIPP liner composite structure.

Table 3. Ring stiffness test results for the group T2.

Sample No.	Loads Corresponding to Pipes with 3.0% Deformation F (N)	3.0% Deformation of the Pipe Corresponding to the Deformation y (mm)	Test Ring Stiffness S_i (kN/m^2)	Bearing Capacity Increment (%)
PE(1) + CIPP(0)	1799.08	10.84	10.7	203.12%
PE(2) + CIPP(0)	3830.2	10.61	23.28	138.77%

As seen in Figure 7, due to the bonding effect, the load–displacement curve of the PE pipe-CIPP liner exhibits multiple descending points (black line in Figure 7). For the non-bonded interface structure of the PE pipe-CIPP liner, with a DR of 21 PE pipe, the overall structure's load–displacement curve is relatively smooth throughout the loading process (red line in Figure 7B), and the interface gap between the PE pipe and the CIPP liner increases with the load. For the PE pipe with a DR of 26, the load–displacement curve of the overall structure is initially smooth, but as deformation intensifies, the top of the PE pipe cracks, causing a descending point on the curve (from E1 (5051.45 N) to E2 (3800.9 N)) (red line in Figure 7A), resulting in a significant gap between the PE pipe and the CIPP liner, although the CIPP liner remains largely undamaged.
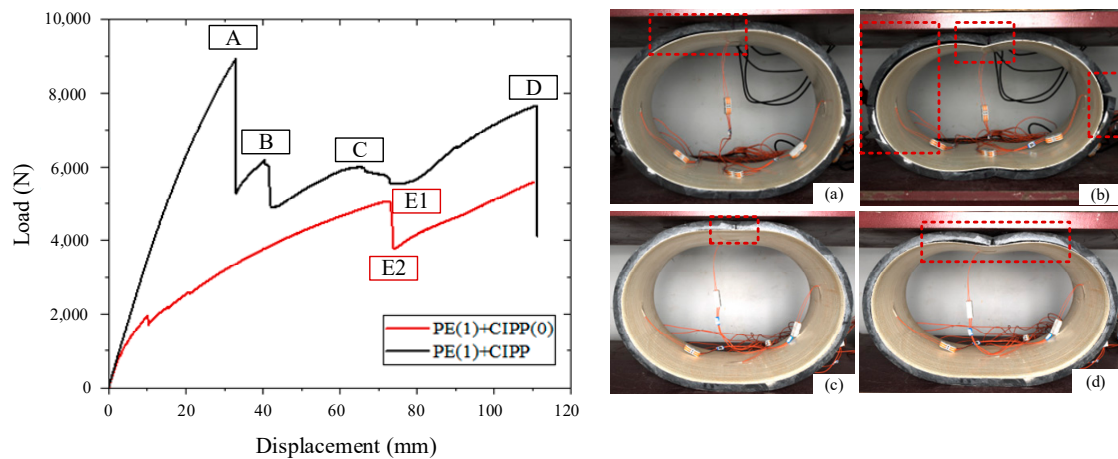
(**A**) DR = 26. (**a**) PE pipe segment failure stage; (**b**) complete specimen failure; (**c**) pipe roof cracking; (**d**) large gap between PE pipe section and CIPP liner
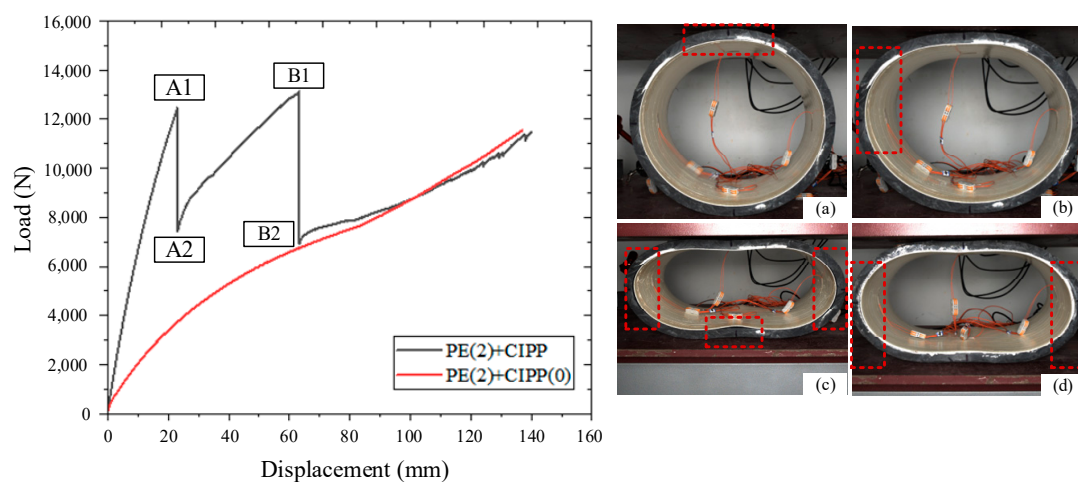
(**B**) DR = 21. (**a**) smaller gaps begin to appear in the interface; (**b**) Interface failure stage; (**c**) CIPP liner failure stage; (**d**) interface gaps to the left and right of the arch line.
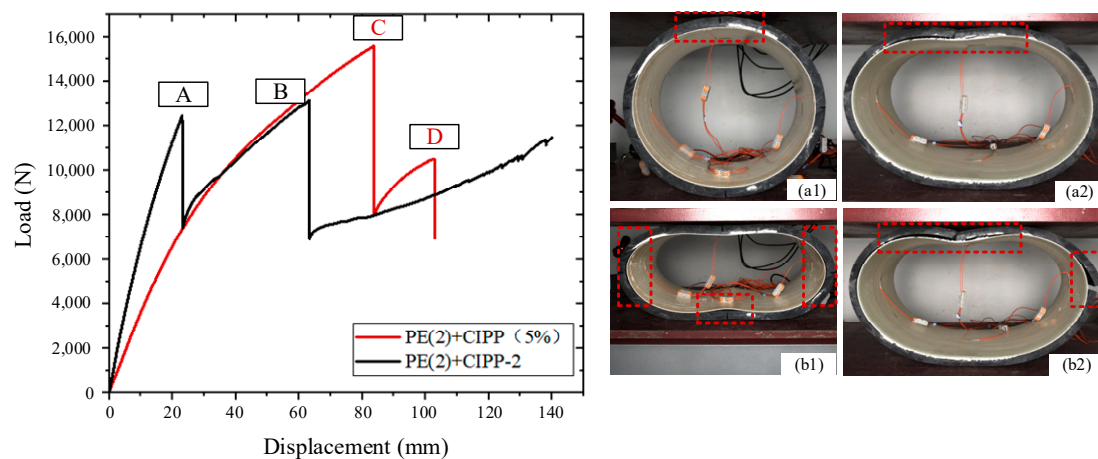
Figure 7. Load-deformation curve of PE pipe–CIPP liner with Different DR.

The ring stiffness is calculated at 3% vertical deformation of the specimen, during which the PE pipe–CIPP liner deforms in harmony, and the bonding effect enhances the overall load-bearing capacity, with the cracking load of the bonded specimen being higher than that of the non-bonded specimen. As the load increases, the interface at the top, bottom, and arch line of the bonded specimen begins to separate, and the overall structure ceases to deform in coordination, reducing its residual load-bearing capacity to the level of the non-bonded specimen. Therefore, the failure of the bonding effect is one of the reasons for the sudden drop in the load-bearing capacity of the composite structure.

3.5. The Effect of Initial Ellipticity on the Bearing Capacity of PE Pipe–CIPP Liner

During the experiment, a steel plate clamp was used to fix the PE pipe with a DR of 21. By controlling the pipe's ovality with a screw, it was compressed to achieve a 5% (20 mm) vertical deformation. After securing it, the CIPP liner was installed, followed by the removal of the steel plate clamp. The end surface of the composite structure specimen was then polished, resulting in a repaired composite structure with an initial ovality.

Figure 8 illustrates the load–displacement curve for the standard and preformed 5% initial ovality PE(2) pipe following CIPP liner. In the first phase of the comparative curve, PE(2) + CIPP-2 exhibits a linear elastic stage from O to A, with the curve's slope gradually decreasing from O to C due to the plastic deformation of the PE pipe segment with initial ovality. The two descending points on the curve correspond to the cracking of the PE pipe. Upon loading to 15,576.01 N, the pipe experienced an 83.7 mm vertical displacement, resulting in the top of the PE pipe cracking (Figure 8(a1)), and the interface between the PE pipe segment and the CIPP liner separating, with the load dropping to 8012.92 N. Continued loading to 10,506.7 N caused the right side of the arch line to fracture, the top crack to widen, and slight protrusions on both sides of the arch line of the CIPP liner (Figure 8(a2)).

Figure 8. Load-deformation curve of PE pipe-CIPP liner with 5% ovality deformation; (**a1**)cracking of PE pipe section specimen at the top of the pipe; (**a2**) slight bulge in CIPP liner at both left and right of arch line; (**b1**) a protruding layer emerged on the inner wall at the right side of the arch line; (**b2**) CIPP liner failure stage.

Figure 9 displays the load-strain curves for three pipe segment specimens: PE(2), PE(2) + CIPP, and PE(2) + CIPP(5). Comparing Figure 9a,b, the strain on the inner and outer walls of the PE pipe specimen was relatively close under the same load, whereas the strain on the outer wall of the PE pipe + CIPP liner was significantly higher than that on the inner wall. This is attributed to the fact that the elastic modulus of the CIPP liner is approximately seven times that of the PE pipe, providing better bending resistance under the same load, resulting in smaller strains. Figure 9c shows that when the composite structure specimen underwent a 20 mm displacement, the strain values at critical points for both the preformed

initial ovality composite structure and the non-preformed ovality composite structure were similar, yet the overall load-bearing performance was lower for the preformed ovality composite structure.
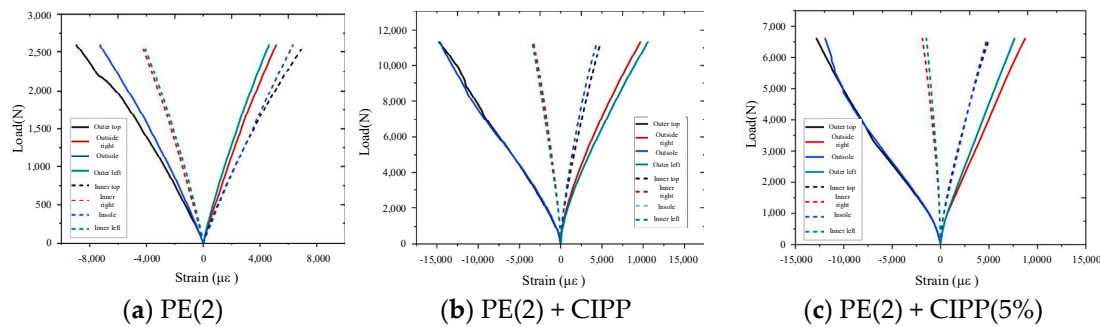

Figure 9. Load-strain curve of the different specimens.

4. Ring Stiffness Prediction Model for PE Pipe–CIPP Liner

The naturally cured CIPP liner, prepared under laboratory conditions, bonds completely with the PE pipe. In the initial load-bearing phase, the composite structure deforms in unison, with the shear strength and tensile bond strength between the liner and the pipe resisting shear and tensile stresses, maintaining a common neutral axis. Consequently, the specimen at this stage can be simplified to a composite curved-beam model (Figure 10). This model comprises two parts, with elastic moduli E_a and E_b, and thicknesses h_a and h_b, respectively. The contact interface is fully bonded, employing the equivalent width method to increase the lower beam width according to the ratio of elastic moduli. Therefore, the ring stiffness of the PE pipe–CIPP liner can be calculated using the following equation:

$$S = \frac{E_a}{D^3} \frac{h_a h_b^3 E_b}{12(E_a h_a + E_b h_b)} \left[4 + 6 \cdot \frac{h_a}{h_b} + 4 \cdot \left(\frac{h_a}{h_b} \right)^2 + \frac{E_a}{E_b} \cdot \left(\frac{h_a}{h_b} \right)^3 + \frac{E_b}{E_a} \cdot \frac{h_b}{h_a} \right] \quad (1)$$

where E_a is the modulus of elasticity of the original pipe; E_b is the modulus of elasticity of the CIPP liner; h_a is the wall thickness of the original pipe; h_b is the wall thickness of the lining; and D is the calculated diameter of the composite structure.
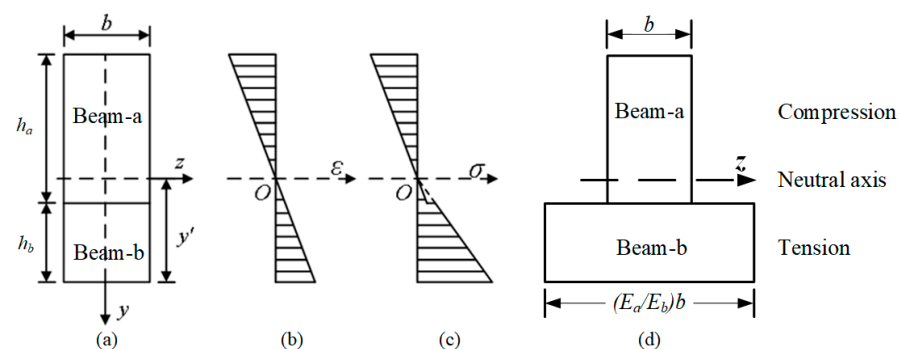

Figure 10. Simplified model of PE pipe–CIPP liner for stacked beams. (**a**) cross-sections of beams a and b; (**b**) bending deformation of beams a and b; (**c**) the neutral axis of the beams a and b; (**d**) combined cross section of beams a and b.

According to the mechanical performance tests of the materials, the elastic modulus of the CIPP liner is 6600 MPa, while the elastic moduli of the three sets of PE pipe segments are 750 MPa, 1050 MPa, and 1000 MPa, respectively. Table 4 presents the theoretical values and experimental results of the ring stiffness of the composite structures calculated using Formula (1). The error between the theoretical and experimental values for PE + CIPP(1) is 2.68%, for PE + CIPP(2) is −9.96%, and for PE + CIPP(3) is −9.26%.

Therefore, this model can reasonably predict the ring stiffness of the repaired PE pipe–CIPP liner composite structure.

Table 4. Theoretical and experimental results of the ring stiffness of the composite structures.

Sample No.	Test Ring Stiffness (kN/m^2)	Calculated Ring Stiffness (kN/m^2)	Error (%)
PE(1) + CIPP	21.98	21.39	2.68%
PE(2) + CIPP	41.18	45.28	−9.96%
PE(2) + CIPP	66.51	72.67	−9.26%

5. Conclusions

This study investigated the failure modes and load-sharing patterns of the repaired PE pipe–CIPP liner composite structure under vertical loading through laboratory experiments. The main findings are summarized as follows:

- CIPP technology significantly enhances the bearing capacity of PE pipe segments, with load increases ranging from 200% to 500%, inversely related to the DR value. The composite structure exhibits distinct load–displacement stages: elastic deformation, interface failure, CIPP liner failure, and brittle fracture of the PE pipe segment concentrated at the top, bottom, and arch line.
- Higher DR values result in lower stiffness, increasing susceptibility to cracking and CIPP liner bulging under load. Initial ovality compromises the composite structure's load-bearing performance, making the original pipe segment more vulnerable to damage.
- Bonded composite structures initially show superior load-bearing capacity compared to tightly fitted structures, although stability decreases post-interface failure, leading to similar ultimate load-bearing capacities.
- The derived ring stiffness calculation formula from the composite beam model accurately predicts ring stiffness for interface-bonded composite materials, aligning well with experimental data.

This study primarily focuses on the bearing characteristics of the PE pipe–CIPP liner composite structure. Future research will investigate how surrounding soil conditions influence the mechanical response of this composite structure under earth pressure and traffic loads.

References

1. Ministry of Housing and Urban Rural Development. *The 14th National Planning for Urban Infrastructure Construction*; MHURD: Beijing, China, 2022.
2. Yu, S.; Park, Y.; Hyun, S.; Park, K. Numerical simulations on shapes and materials and deterioration model of flexible sewer systems. *Desalination Water Treat.* **2015**, *54*, 1290–1298. [CrossRef]
3. Spangler, M.G. *The Structural Design of Flexible Pipe Culverts*; Iowa Engineering Experiment Station: Ames, IA, USA, 1941.
4. Watkins, R.K.; Spangler, M.G. Some characteristics of the modulus of passive resistance of soil: A study in similitude. In Proceedings of the Thirty-Seventh Annual Meeting of the Highway Research Board, Washington, DC, USA, 6–10 January 1958.
5. Spangler, M.G. *Soil Engineering*, 4th ed.; Harper & Row: Manhattan, NY, USA, 1982.
6. Howard, A.K. The USBR Equation for Predicting Flexible Pipe Deflection. *Int. J. Quantum Chem.* **1981**, *3*, 21–27.

7. Jeyapalan, J.K.; Boldon, B.A. Performance and Selection of Rigid and Flexible Pipes. *J. Transp. Eng.* **1986**, *112*, 507–524. [CrossRef]

8. Jeyapalan, J.K.; Ethiyajeevakaruna, S.W.; Boldon, B.A. Behavior and design of buried very flexible plastic pipes. *J. Transp. Eng.* **1987**, *113*, 642–657. [CrossRef]

9. Cholewa, J.A.; Brachman, R.W.I.; Moore, I.D. Response of a polyvinyl chloride water pipe when transverse to an underlying pipe replaced by pipe bursting. *Can. Geotech. J.* **2009**, *46*, 1258–1266. [CrossRef]

10. Saiyar, M.; Ni, P.; Take, W.A.; Moore, I.D. Response of pipelines of differing flexural stiffness to normal faulting. *Géotechnique* **2016**, *66*, 275–286. [CrossRef]

11. Ni, P.; Mangalathu, S.; Yi, Y. Fragility analysis of continuous pipelines subjected to transverse permanent ground deformation. *Soils Found.* **2018**, *58*, 1400–1413. [CrossRef]

12. Liu, J.; Xie, Q.; Ye, M.; Ni, P.; Qin, X. Response of UPVC pipes buried in sand under lateral ground movement. *Tunn. Undergr. Space Technol.* **2023**, *138*, 105177. [CrossRef]

13. Takahashi, Y.; Deguchi, T.; Li, L.; Yamada, K. A Study on the Bedding Effects of the Deteriorated Existing Pipe on the Flexible Rehabilitated Pipe and its Mechanism. *J. Jpn. Sew. Work. Assoc.* **2002**, *39*, 103–115.

14. Gumbel, J.; Spasojevic, A.; Mair, R. Centrifuge modelling of soil load transfer to flexible sewer liners. In *New Pipeline Technologies, Security, and Safety*; American Society of Civil Engineers: Reston, VA, USA, 2003; pp. 352–362.

15. Hsu, J.M.; Shou, K.J. Experimental study of the separated joint of an underground pipeline rehabilitated by cured-in-place pipe. *Undergr. Space* **2022**, *7*, 543–563. [CrossRef]

16. Allouche, E.; Alam, S.; Simicevic, J.; Sterling, R.; Condit, W.; Matthews, J.; Selvakumar, A. A pilot study for retrospective evaluation of cured-in-place pipe (CIPP) rehabilitation of municipal gravity sewers. *Tunn. Undergr. Space Technol.* **2014**, *39*, 82–93. [CrossRef]

17. Zhang, X.; Fang, H.; Hu, Q.; Ma, B.; Hu, S.; Du, M.; Du, X.; Yang, K.; Li, B.; Shi, M. Mechanical performance of corroded reinforced concrete pipelines rehabilitated with sprayed-on cementitious liners subjected to combined loads. *Tunn. Undergr. Space Technol.* **2022**, *120*, 104266. [CrossRef]

18. Argyrou, C.; Bouziou, D.; O'Rourke, T.D.; Stewart, H.E. Retrofitting pipelines with cured-in-place linings for earthquake-induced ground deformations. *Soil Dyn. Earthq. Eng.* **2018**, *115*, 156–168. [CrossRef]

19. Shou, K.J.; Huang, C.C. Numerical analysis of straight and curved underground pipeline performance after rehabilitation by cured-in-place method. *Undergr. Space* **2020**, *5*, 30–42. [CrossRef]

20. Yang, K.; Fang, H.; Zhang, X.; Li, B.; Hu, Q. Investigation of mechanical properties of corroded concrete pipes after cured-in-place-pipe (CIPP) rehabilitation under multi-field coupling. *Tunn. Undergr. Space Technol.* **2022**, *128*, 104656. [CrossRef]

21. Mogielski, K.A.; Kuliczkowski, A.; Kuliczkowska, E. Change in Toughness Parameters of Sewer Pipes Rehabilitated with Two Types of Epoxy CIPP Liners. *J. Pipeline Syst. Eng. Pract.* **2017**, *8*, 04017015. [CrossRef]

22. Kuliczkowski, A.; Mogielski, K. Results of laboratory tests of concrete, vitrified clay and PVC sewer pipes with CIPP liners. *Struct. Environ.* **2012**, *4*, 23–34.

23. Hu, H.; Niu, F.; Dou, T.; Zhang, H. Rehabilitation effect evaluation of CFRP-lined prestressed concrete cylinder pipe under combined loads using numerical simulation. *Math. Probl. Eng.* **2018**, *2018*, 3268962. [CrossRef]

24. Yan, X.; Deng, C.; Zhao, Y.; Liu, H.; Mei, S. Mechanical Performance Study of Pipe-Liner Composite Structure Based on the Digital Image Correlation Method. *IEEE Trans. Instrum. Meas.* **2022**, *72*, 3504212. [CrossRef]

25. *ISO 4427-2:2019*; Plastics piping systems for water supply, and for drainage and sewerage under pressure—Polyethylene (PE)—Part 2: Pipes. International Organization for Standardization: Geneva, Switzerland, 2019.

26. *ISO 11295:2022*; Plastics piping systems used for the rehabilitation of pipelines—Classification and overview of strategic, tactical and operational activities. International Organization for Standardization: Geneva, Switzerland, 2022.

27. *ISO 11296-3:2018*; Plastics piping systems for renovation of underground non-pressure drainage and sewerage networks—Part 3: Lining with a cured-in-place pipe. International Organization for Standardization: Geneva, Switzerland, 2018.